



# Removal kinetics of stearic acid discrete deposits on photocatalytic self-cleaning surfaces: Effect of deposit initial size distribution

David Ollis

*Chemical and Biomolecular Engineering, North Carolina State University, Raleigh, NC 27695-7905, United States*

## ARTICLE INFO

### Article history:

Received 18 October 2016

Received in revised form

15 December 2016

Accepted 7 February 2017

Available online 9 February 2017

### Keywords:

Photocatalysis

Self-cleaning

Stearic acid

Kinetics

Models

## ABSTRACT

Earlier reports by Sawunyama et al. (1997, 1999) and Ghazzal et al. (2011) used atomic force microscopy (AFM) and optical microscopy to characterize the structure of stearic acid (SA) deposits on polycrystalline TiO<sub>2</sub> films and Ti [110] crystal surfaces. Their preparation methods and catalysts yielded island-like SA deposits, rather than continuous films, for stearic acid submonolayers and multi-layers. Ghazzal observed that individual islands showed disappearance kinetics to be zero order with respect to island area, but apparently first order with respect to total SA remaining.

We develop here kinetic models which are consistent with these “island” findings and establish the guidelines for apparent kinetic order of reaction, n:

1. Island deposits of a single size will exhibit apparent zero order kinetics., n = 0.
2. Island deposits with a narrow distribution of island sizes will exhibit an apparent half order behavior, n = 0.5.
3. Island deposits with a broad size distribution will exhibit an apparent reaction order of unity, n = 1.

Our conclusion is that meaningful kinetic analysis of SA island photocatalyzed disappearance, and thus that of any oxidizable, carbonaceous pollutant which deposits in island form, rather than as a continuous film, requires knowledge of the initial island size distribution. The SA deposits may also undergo significant rearrangement as the titania surface is illuminated, quickly transforming the latter from hydrophobic to hydrophilic. Thus it is the reactant film and/or island distribution after initiation of illumination which is most relevant to kinetic modeling attempts.

© 2017 Elsevier B.V. All rights reserved.

## 1. Introduction

### 1.1. Stearic acid: continuous thin film assumption

Stearic acid( $\text{CH}_3(\text{CH}_2)_{16}\text{COOH}$ ) multilayer films deposited on dense, **non-porous or microporous ( $\text{dp} < 1\text{--}2 \text{ nm}$ )** titania photocatalyst layers have been shown numerous times to exhibit intrinsic zero order removal kinetics as established first by Paz et al. [1] and later confirmed by Mills et al. [2], Allain et al. [3]. Peruchon et al. [4] also reported the zero order removal of stearic acid from titania-based non-porous, commercial self-cleaning glasses. (We note that FTIR measurements, used in all four studies [1–4], track the  $-\text{CH}_2-$  group which serves as a convenient surrogate reactant for stearic acid oxidative removal. As these methylene groups are also found in many of the intermediates arising and disappearing in the course of stearic acid conversion to CO<sub>2</sub>, the FTIR data widely

used in photocatalysis studies, because of its convenience in measurement, does not represent mechanistically the fundamental rate of SA oxidation itself.

Similar zero order results were found with other measurement techniques and other long chain fatty acids as reactants. Thus Romeas et al. [5] showed zero order mass removal for palmitic acid ( $\text{CH}_3(\text{CH}_2)_{14}\text{COOH}$ ) deposited on TiO<sub>2</sub>, and Zaleska et al. [6] studied lauric acid ( $\text{CH}_3(\text{CH}_2)_{10}\text{COOH}$ ) on single crystal anatase, finding zero order decrease of multi-layer lauric acid surface coverage.

However, when stearic acid was deposited on thicker, **mesoporous ( $\text{dp} > 5 \text{ nm}$ )** TiO<sub>2</sub> films, both Mills et al. [2] and Allain et al. [3] reported apparent first order kinetics of  $-\text{CH}_2-$  film removal. We have shown with kinetic models that an oxidizable multi-layer reactant, distributed uniformly throughout a (meso)porous, optically thick photocatalyst, exhibits an apparent first order kinetic rate of organic film removal [7]. This kinetic order disguise is due to diminution with depth of local irradiance, and thus rate constant, because of photocatalyst absorption of bandgap or shorter wavelengths.

E-mail address: [ollis@ncsu.edu](mailto:ollis@ncsu.edu)

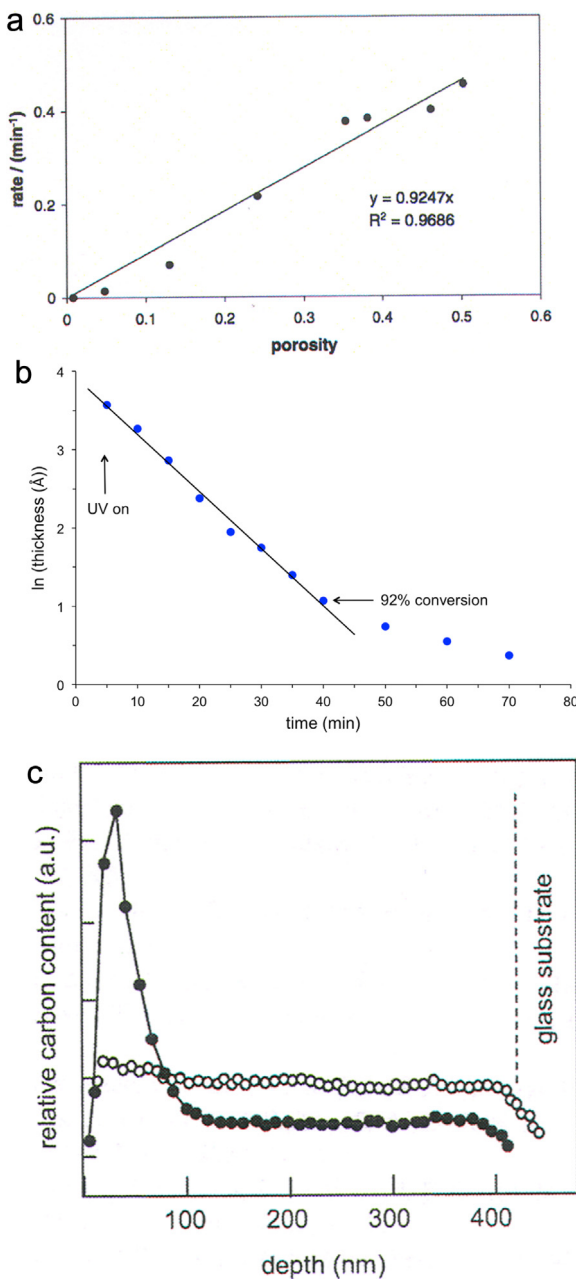


**Fig. 1.** (a) Rate of reaction vs. calculated porosity of titania thick film (Reprinted by permission of Springer) [8]. (b) Semilog plot of data for predicted stearic acid film thickness within a porous titania layer. Data from Fig. 11c calculated curve of Remillard et al. [9]. (c) SIMS profile of the carbon content for a microporous (filled circles) and mesoporous (open circles) films on which 1.5  $\mu\text{g}/\text{cm}^2$  stearic acid was deposited [3] (Reprinted by permission of Wiley-VCH).

Our porous photocatalyst model assumed uniform initial distribution of reactant stearic acid with a zero order local removal rate at all times, until local exhaustions of stearic acid, and demonstrated an apparent first order behavior for such non-uniformly illuminated circumstances [7]. Support for this assumption of uniform stearic acid distribution within a mesoporous photocatalyst is found in reports by Mills et al. [8] and Remillard et al. [9]. The former FTIR study demonstrated a strong correlation between overall rate of reaction and photocatalyst porosity (Fig. 1a), while ellipsometry data from the latter for calculated SA film thickness within a porous catalyst show clear first order behavior for SA disappearance (Fig. 1b), a confirmation of the kinetic disguise modeled earlier for porous photocatalysts [7]. A third example is demonstrated by Allain et al. [3] in Fig. 1c showing that a microporous catalyst has

stearic acid predominantly at the surface, whereas the mesoporous catalyst shows carbon initially uniformly distributed throughout the depth of the photocatalyst, as assumed in our previous analysis [7].

Thus, kinetic models corresponding to removal of uniformly deposited, continuous fatty acid layers for porous and non-porous photocatalysts appear to be validated experimentally and in suitable kinetic models.

## 1.2. Stearic acid: discrete island evidence

Sawunyama et al. [10,11] and Ghazzal et al. [12] have studied sub-monolayer, monolayer, and multi-layer deposits of stearic acid on non-porous surfaces, finding that, either initially or upon illumi-

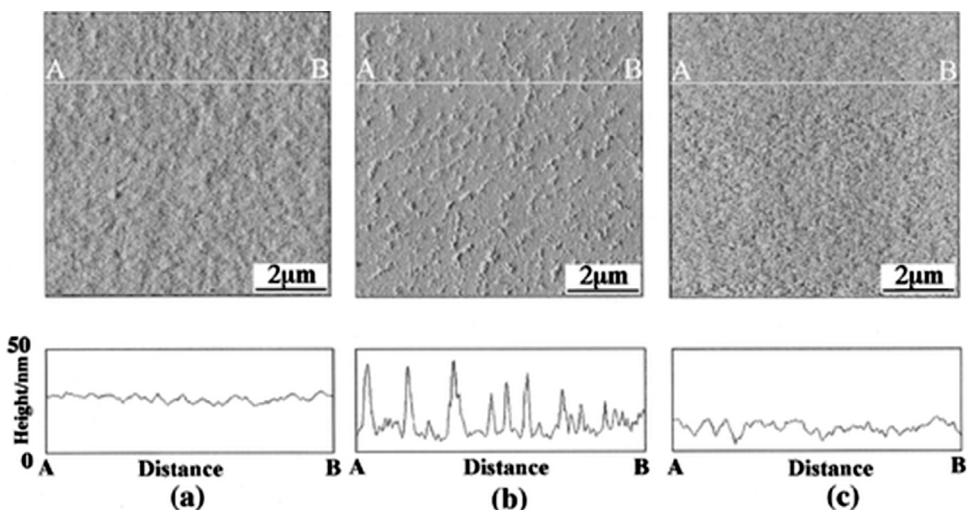


**Fig. 2.** Low-resolution AFM images and the corresponding topographic cross-sectional profiles for the photocatalyzed oxidation of a five-layer stearic acid Langmuir-Blodgett deposit on an anatase TiO<sub>2</sub> film. Images were obtained after (a) 0, (b) 10, and (c) 60 min. of irradiation, respectively. Note transition from a continuous SA deposit (a) to a distribution of discrete deposits (b) and finally achievement of a clean, SA-free surface. [11] (Reprinted by permission of ACS).

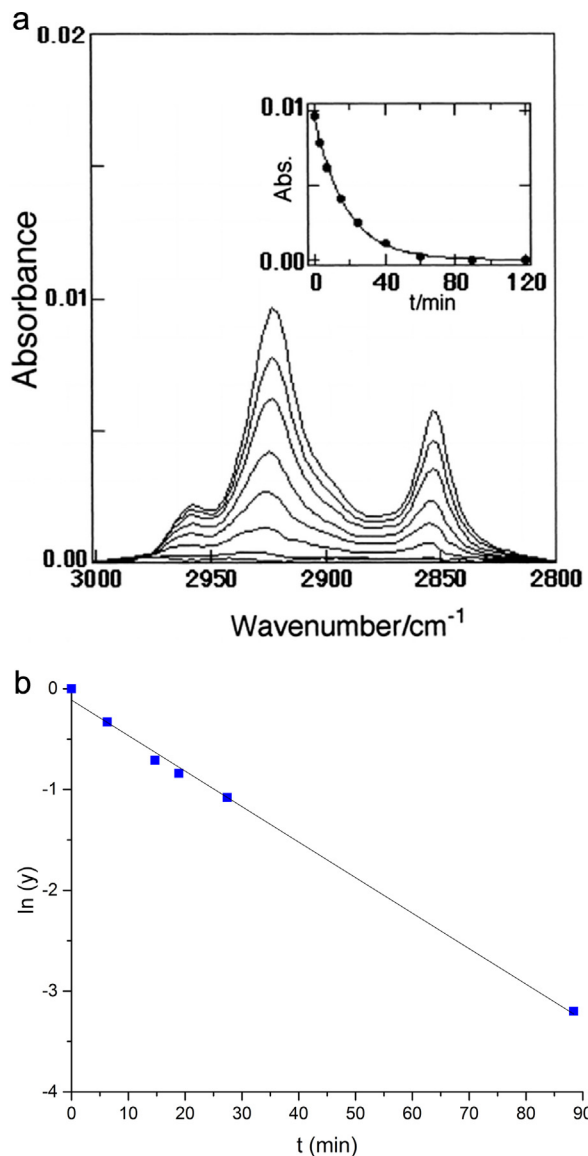


**Fig. 3.** (a) FTIR spectra for the photodecomposition of a five-layer stearic acid LB film mediated by anatase TiO<sub>2</sub> film. The spectra were recorded after 0, 3, 7, 15, 25, 40, 60, 90, and 120 min of irradiation, respectively. The inset shows a plot of absorbance (CH<sub>2</sub> asymmetric stretch, 2922.8 cm<sup>-1</sup>) as a function of irradiation time. (Reprinted by permission of ACS) [11]. (b) Semi-log plot of data from inset in Fig. 3a, establishing first order behavior over first 90 min of irradiation.

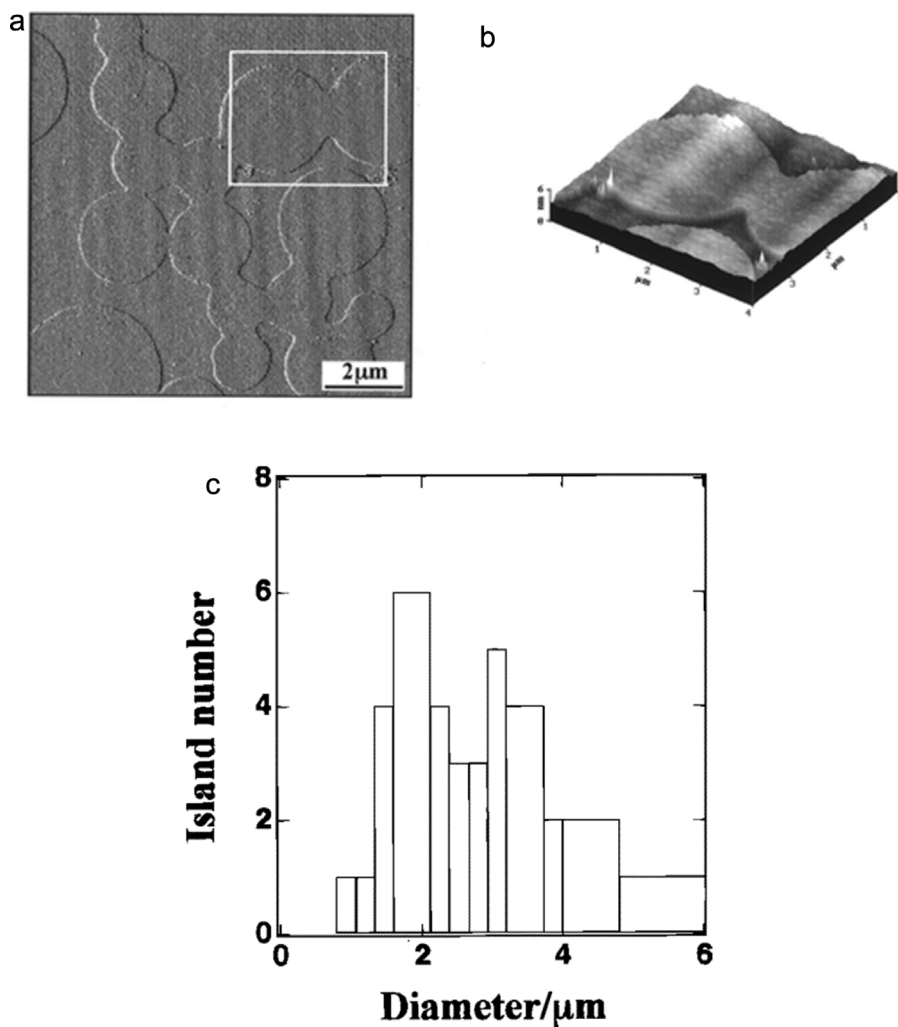


**Fig. 4.** (a) Typical AFM image of a partial monolayer of stearic acid on a rutile  $\text{TiO}_2$  [110] surface. Distinctive features include the sizes and circular shapes of the coalesced domains. (b) Three dimensional image of the island framed in Fig. 3a. The partial monolayer film was transferred at a surface pressure of  $15 \text{ nm m}^{-1}$  at  $20^\circ\text{C}$ . (Reprinted with permission of ACS) [10]. (c) Island size distribution obtained by visually counting islands of a given size. The bulk of the islands had diameters in the range of  $1\text{--}4 \mu\text{m}$  (Reprinted by permission of ACS) [10].

nation, island-like stearic acid structures are observed. As Ghazzal noted, these were new SA configurations. As our earlier analyses [7] of stearic acid removal considered only continuous films, these novel island structures required a new analysis to explain the apparent first order kinetics on such non-porous surfaces.

To create new kinetic models for island configurations, we briefly review the earlier island studies to quantify the initial reactant configurations and develop local intrinsic reaction rate expressions. We show quantitatively how these local rate forms can lead to an apparent positive reaction order,  $n > 0$ , whose value depends upon the breadth of the initial island size distribution in the original deposit.

Sawunyama et al. [10] first created stearic acid multilayers deposited on polycrystalline titania as a uniform, Langmuir-Blodgett multi-layer of about 15 nm thickness (Fig. 2a – Fig 2c). Upon illumination, a highly non-uniform profile developed (Fig. 2b), implying a deposit rearrangement yielding discrete features of width the order of  $0.1\text{--}1.0 \mu\text{m}$ , and heights at times clearly greater than the initial, uniform film thickness (Compare Fig. 2a and b). This rearrangement was consistent with a transition from a continuous film to discrete, if at time connected, structures. The known

hydrophobic to hydrophilic transition for titania photocatalyst surfaces, which occurs upon nUV illumination, may have catalyzed this stearic acid layer transformation

Their overall photocatalyzed reaction rates were first order (Fig. 3a,b), in contrast to prior zero order results for SA on other non-porous titania surfaces reported by Paz [1], Mills [2], Allain [3], and Peruchon [4]. As reaction progressed, a uniform surface profile was eventually recovered, now presumably cleared of most or all stearic acid SA and reaction products, and of a relatively constant height, as shown in Fig. 3c. Sawunyama et al. [10] proposed that a catalytically non-uniform surface was responsible, with a reaction rate variation due to local activity variation.

These authors subsequently studied monolayer and submonolayer SA deposits on  $\text{TiO}_2$  rutile [110] single crystals [11]. Here, atomic force microscopy (AFM) revealed the initial submonolayer SA deposits on their non-porous rutile [110] crystal to be round island structures (Fig. 4a,b). As reaction proceeded, holes appeared in the island-like structures, and grew continuously, while the island size appeared to remain constant.

The initial SA deposit was also characterized as a distribution of island diameters, shown in Fig. 4c. Island diameters ranged from

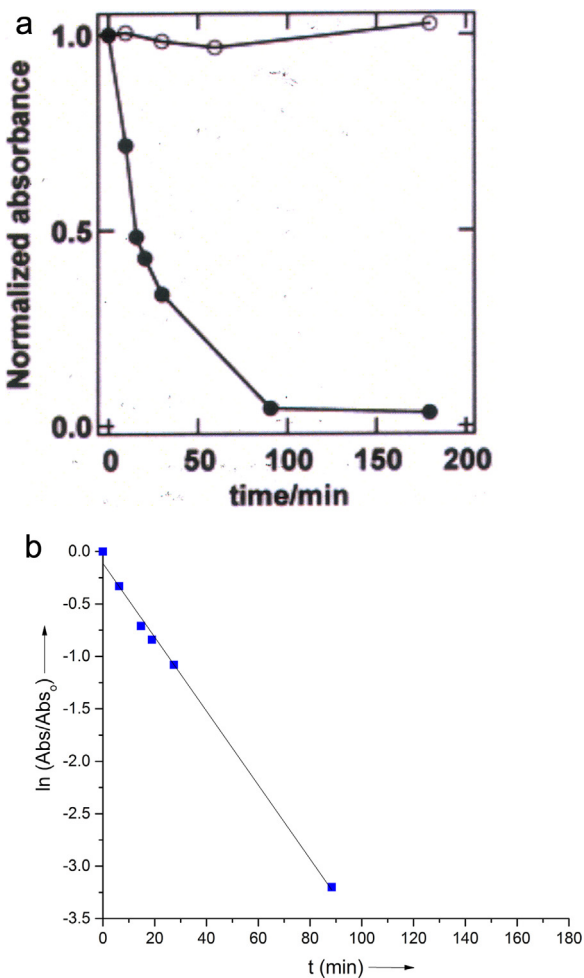


**Fig. 5.** (a) Normalized absorbance versus time profiles for monolayer of stearic acid on TiO<sub>2</sub> [110] (solid circles) and CaF<sub>2</sub> (open circles) with UV irradiation time, respectively (Incident UV light irradiance = 2.5 mW cm<sup>-2</sup>). The spectra were recorded at 0, 10, 15, 20, 30, 90, and 120 min, respectively (Reprinted with permission of ACS) [10]. (b) Semilog plot of Fig. 5a data for TiO<sub>2</sub> photocatalyzed oxidation of stearic acid monolayer showing apparent first order disappearance.

about 1 μm to 5–6 μm, corresponding to about a 25–36 fold island area variation from smallest to largest. The uniformly circular structure on rutile [110] also suggests a two dimensional, liquid-like behavior and relatively weak (titania-stearic acid) binding so that surface tension driven rearrangement is dominant.

The global rate of photocatalyzed reaction was followed via FTIR. Their data of Fig. 5a [10] displays apparent first order behavior, as shown by their data replotted in Fig. 5b.

More recently, a yet different fatty acid deposit configuration was found by Zaleska et al. [6] who studied lauric acid ( $\text{CH}(\text{CH}_2)_{10}\text{COOH}$ ) multilayers on anatase single crystals of unstated orientation. A ridge-like structure existed initially (Fig. 6a). As photocatalyzed reaction began, these deposits exhibited a thinning evolution (Fig. 6b) as nearly parallel ridges and valleys, with valley and ridge widths of the order of microns. Here there is clearly a non-uniformly coated surface and a substantial interaction strength of lauric acid with the local surface. Over time, the ridges became narrower, but their height stayed nearly constant as the reaction extent progressed (Fig. 6b). The initial ridges are the order of 5–10 μm in width, and a ridge height the order 70 nm is retained until near the end of SA removal (Fig. 6b). Oxidative attack of these ridges was preferential: material removal occurred almost exclusively at the left side of the deposits shown (Fig. 6b). The kinetics of SA removal were measured as the percent of the

viewed surface which was free of LA. A zero order dependence is evident in Fig. 6c [6]

Ghazzal et al. [12] used AFM and optical microscopy to explore the semi-crystalline stearic acid islands which formed on a TiO<sub>2</sub> polycrystalline film (Fig. 7a,b). They found that, under UV illumination, these irregular islands grew both smaller in area and thinner as well, illustrated by the inset photos of Fig. 8a. Using optical microscopy, they recorded island area sizes vs time, finding that islands of similar initial area and height disappeared at a rate which was zero order in island projected area,  $a$  (Fig. 8b). Thus, for an island of area  $a$ ,

$$\frac{da}{dt} = -k, \quad (1)$$

regardless of island size, at least for the two-fold variation in size in Fig. 8b. A zero order result was also noted for islands of different initial heights.

Notwithstanding the kinetics of individual island disappearance, Ghazzal et al. [12] note an apparent first order global disappearance of IR signal (Fig. 9a). Their data replotted in Fig. 9b shows confirmation of first order behavior: linear  $\ln(\text{Abs}/\text{Abs}_0)$  vs time plots. Analysis in the next section shows such behavior is expected when a relatively broad distribution of island sizes is initially present.

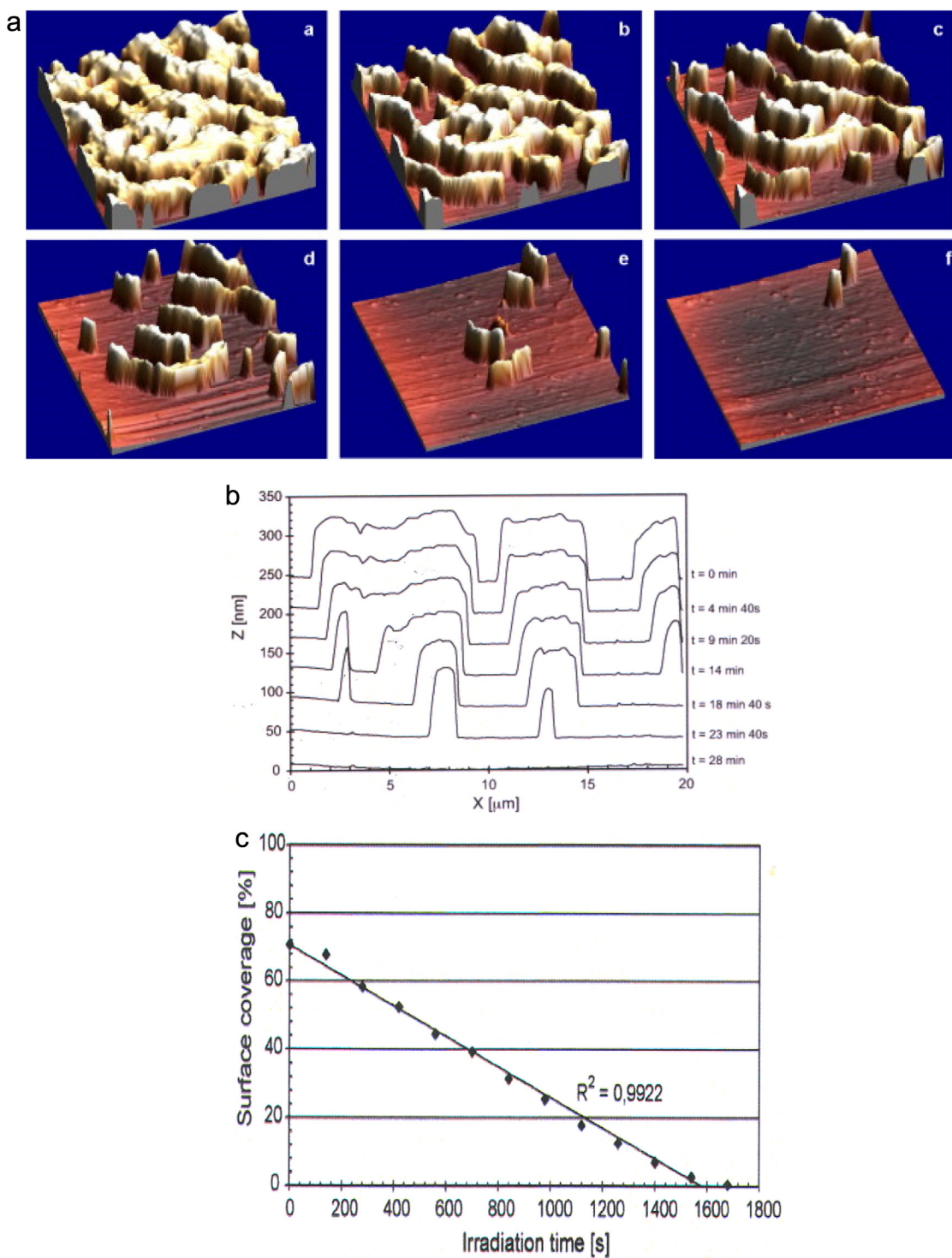


**Fig. 6.** (a) Sequential AFM images ( $20 \mu\text{m} \times 20 \mu\text{m}$ ) of the anatase-catalyzed photocatalytic oxidation of lauric acid film (a) before irradiation; after (b) 11 min 40 s; (c) 16 min 20 s; (d) 21 min; (e) 25 min 40 s; and (f) 28 min of irradiation (Reprinted with permission of Elsevier) [6]. (b) Cross-sectional profiles showing the surface morphology of a thin film of lauric acid on an anatase single crystal at different stages of degradation (a) AFM image ( $20 \mu\text{m} \times 20 \mu\text{m}$ ) showing position of cross-sectional profile (b)) [6]. (c) Surface coverage vs. time for photocatalyzed destruction of lauric acid deposited on an anatase single crystal surface. [6] Note apparent zero order kinetics (Reprinted by permission of Elsevier).

## 2. Analysis

To analyze these prior kinetic results, we model the process of photocatalyzed SA islands for three initial size distributions: monodisperse, narrow, and broad.

### 2.1. Monodisperse island distribution

The individual islands disappear according to the zero order model of Eq. (1) as reported by Ghazzal [12]:

$$\frac{da}{dt} = -k$$

If all SA is deposited in the form of  $N$  islands of the same individual area, then the rate of total area,  $A(t)$ , reduction would be given by Eq. (2):

$$\frac{dA(t)}{dt} = N \frac{da}{dt} = -Nk, \quad (2)$$

providing the integrated result:

$$A(t) = N a(t) = N a(0) - Nkt = A(0) - Nkt$$

which predicts zero order total area kinetics, and disappearance of all islands at time  $t'$  when

$$t' = a(0)/k. \quad (3)$$

### 2.2. Narrow island distribution

We suppose a narrow distribution of island areas having, for example, a five-fold area variation and a uniform size distribution, and consider a population of five islands with sizes which are integer multiples of area  $a$ :

$$a_1 = a, a_2 = 2a; a_3 = 3a; a_4 = 4a, \text{ and } a_5 = 5a. \quad (4)$$

Then the smallest island vanishes when  $t = a/k$ , the next when  $t = 2a/k$ , the third at  $t = 3a/k$ , etc, and the last at  $t = 5a/k$ . We have assumed here that  $k$  is independent of island size, as suggested by the identical slopes in Fig. 8b.

The total island area,  $A(t)$ , at any time  $t$  is thus

$$A(t) = (a_1 + a_2 + a_3 + a_4 + a_5)$$

$$= (a + 2a + 3a + 4a + 5a) - 5kt \quad \text{for } 0 < t < a/k. \quad (5a)$$

$$= (2a + 3a + 4a + 5a) - 4kt \quad \text{for } a/k < t < 2a/k \quad (5b)$$

$$= (3a + 4a + 5a) - 3kt \quad \text{for } 2a/k < t < 3a/k \quad (5c)$$

$$= (4a + 5a) - 2kt \quad \text{for } 3a/k < t < 4a/k \quad (5d)$$

$$= (5a) - kt \quad \text{for } 4a/k < t < 5a/k \quad (5e)$$

$$\text{and } = 0 \quad \text{for } t > 5a/k \quad (5f)$$

This set of equations produce five line segments of progressively smaller slopes ( $=-5k, -4k, \text{ etc}$ ) to represent  $A(t)$  vs time. We demonstrate via trial and error the apparent kinetic order for  $A$  disappearance by assuming zero, half, and first order behavior, thus

Order assumed:

$$(\text{zero}) \frac{dA}{dt} = -kt \Rightarrow A(t) = A(0) - kt \quad (6a)$$

$$(\text{half}) \frac{dA}{dt} = -k'A^{0.5} \Rightarrow A(t)^{0.5} = A(0)^{0.5} - 2kt \quad (6b)$$

$$(\text{first}) \frac{dA}{dt} = -k''A \Rightarrow \ln\{A(t)\} = \ln A(0) - k''t \quad (6c)$$

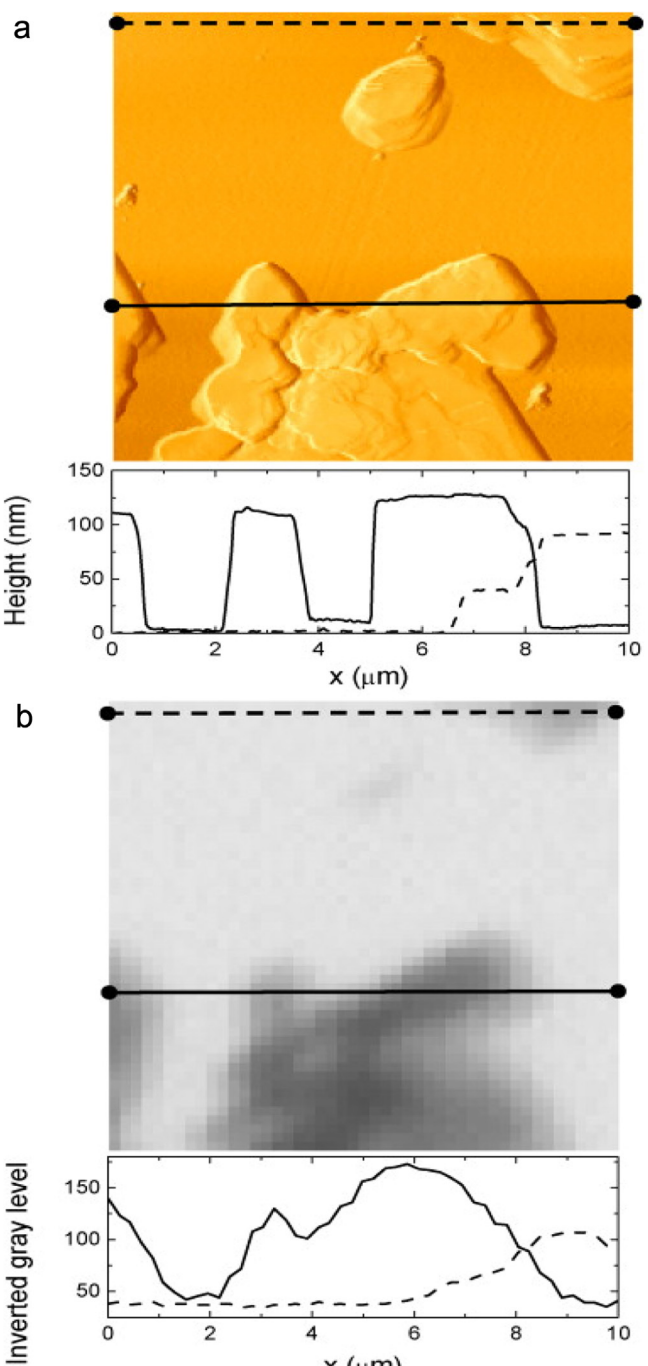


**Fig. 7.** (a) Representative (10 μm x 10 μm) AFM image of the SA-coated titania film with two height profiles below corresponding to the dashed and solid horizontal lines on the image. (b) Optical microscopy image of the same region of the SA-coated titania film with two inverted gray level profiles corresponding to the dashed and solid horizontal lines at exactly the same location as those in Fig. 7a (Reprinted by permission of Elsevier) [12].

These integrated equations show that we can test for the apparent kinetic order generated by the model: for zero order,  $A(t)$  is linear in time, for half order,  $A(t)^{0.5}$  will be linear in time, and for first order,  $\ln\{A(t)\}$  will vary linearly with time.

Using Eqs. (5a)–(5f), we calculated the area remaining when  $t/(a/k) = 1, 2, 3, 4, \text{ and } 5$ , and plotted the results in Fig. 10 assuming zero, half, and first order global behavior for  $A(t)$  vs time. The half order rate form of  $A(t)^{0.5}$  provides the best approximation of reaction order up to about 93% conversion.

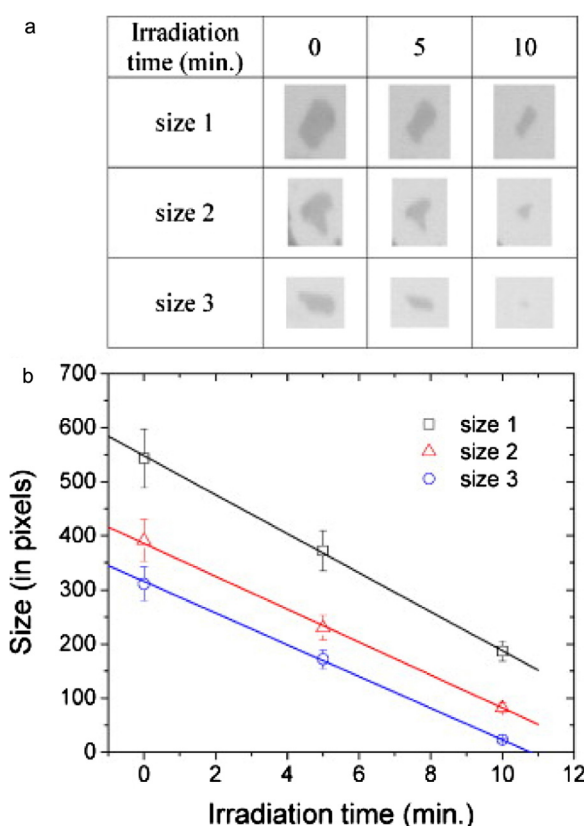


**Fig. 8.** (a) Evolution of three islands showing comparable heights and different initial sizes (size 1 > size 2 > size 3) as a function of UV-irradiation time. (b) Size of the islands as a function of UV-irradiation time (Reprinted by permission of Elsevier) [12].

### 2.3. Broad size distribution

We assume the broader and non-uniform size distribution of island areas (25–30 fold variation) (Fig. 4c) found by Sawunyama et al. [10] for stearic acid deposits on single crystal [110]  $\text{TiO}_2$  surface. Using the same island kinetic treatment as above, now including the non-uniform size distribution of island number  $n(i)$  for each area size  $a(i)$ , gives a total area at any time  $t$ ,  $A(t)$ :

$$A(t) = \sum n(i) a(i)$$

$$= \sum n(i) [a(i, 0) - k] t.$$

Taking the size distribution for  $n(i)$  from that observed by Sawunyama et al. (Fig. 4c) [10], and calculating  $A(t)$  vs time provides a very good apparent first order fit (Fig. 11). This accord rationalizes the observed first order behavior noted by Sawunyama [10,11], and provides a quantitative validation of the earlier first order suggestion of Ghazzal [12].

### 3. Conclusion

The apparent kinetic order of stearic acid island removal from non-porous  $\text{TiO}_2$  surfaces provides strong kinetic disguises which are dependent on initial island size distribution:

Monodispersed islands give zero order kinetics.

A narrow, uniform area size distribution (a–5a) gives apparent half order kinetics

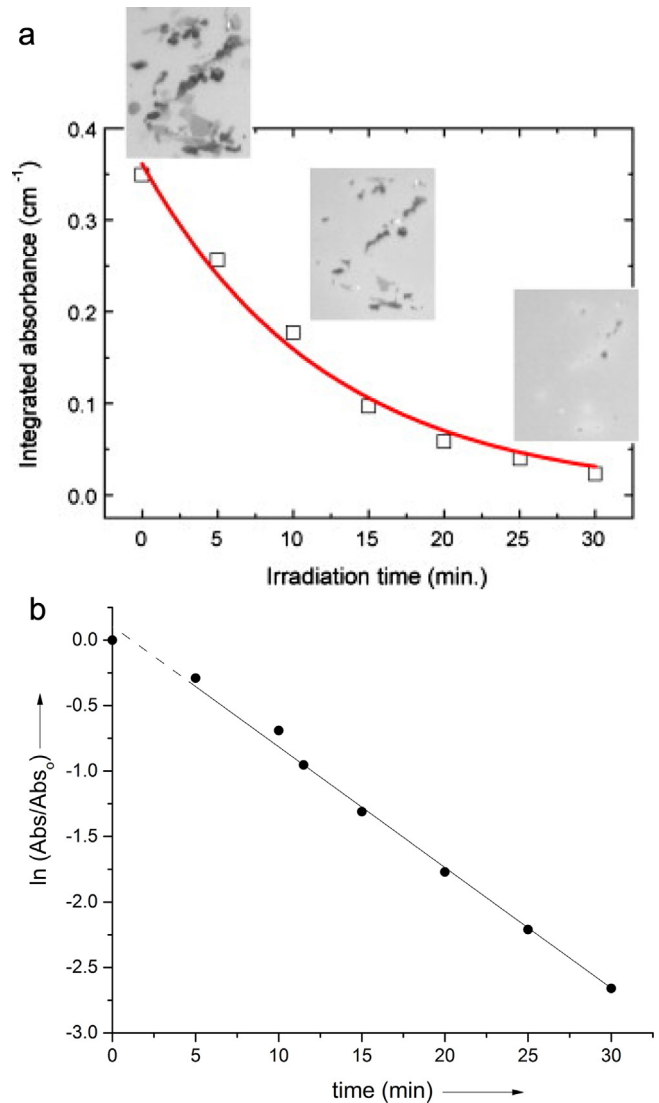


**Fig. 9.** (a) Integrated IR absorbance from  $2700 \text{ cm}^{-1}$  to  $3000 \text{ cm}^{-1}$  of the SA coated titania film as a function of UV-irradiation. The images on the graph show the SA coating aspect at different irradiation times [12] (Reprinted by permission of Elsevier). (b) Semilog plot of Fig. 9a data verifying the first order behavior of the overall rate of reaction.

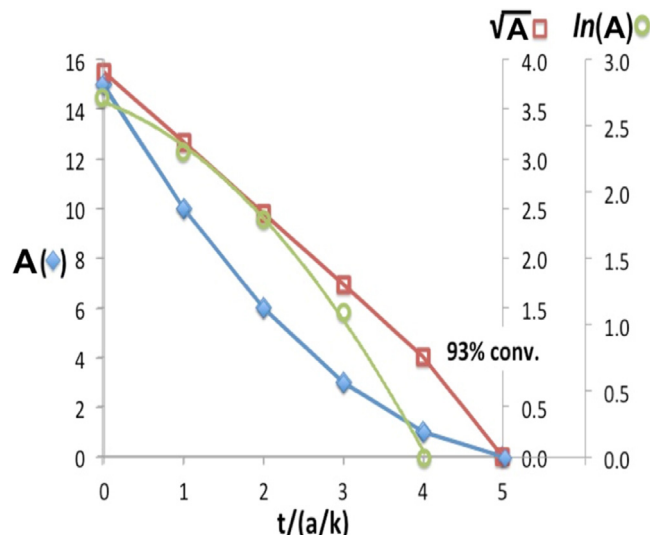


**Fig. 10.** Kinetic order test: Plots of calculated  $A(t)$ ,  $[A(t)]^{0.5}$ , and  $\ln[A(t)]$  vs time from text models for zero, half, and first order reactions, respectively. The half order model exhibits linearity for conversion up to 93%, thus  $n = 0.5$  for this circumstance.

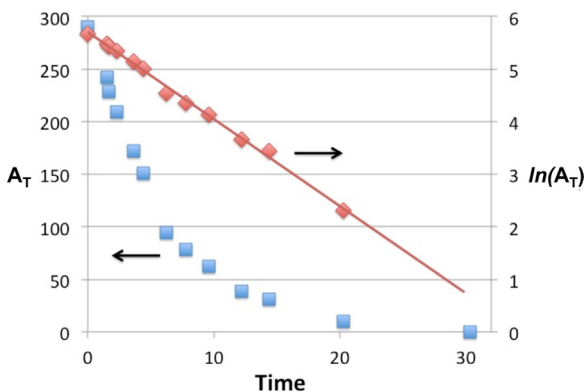


**Fig. 11.** Plots of calculated total area  $A$  as  $A(t)$  vs time, and as  $\ln[A(t)]$  vs time. The linearity of the semilog plot indicates an apparent first order reaction,  $n = 1$ .

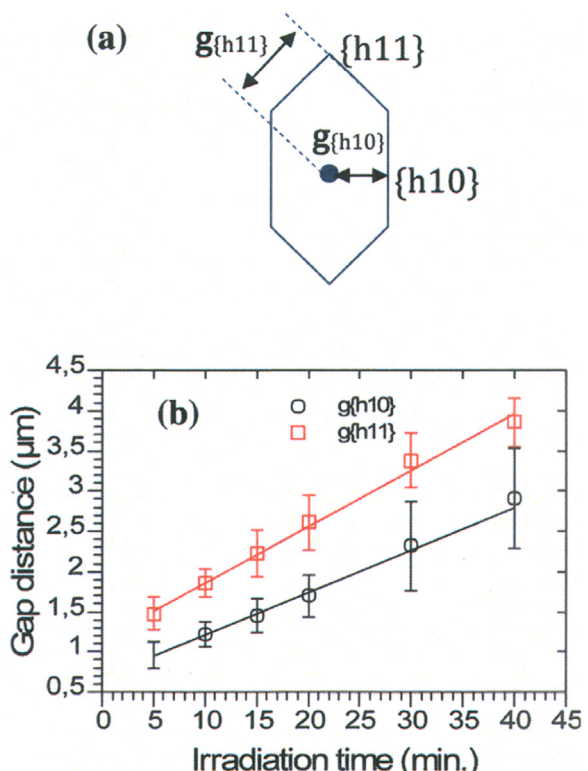


**Fig. 12.** (a) Definition of the gap distances  $g\{h11\}$  and  $g\{h10\}$  between the active microdomain (anatase, center) and the edges of the pits in a stearic acid single crystal according to the  $\{h11\}$  and  $\{h01\}$  faces, respectively, and (b) their evolution as a function of ultraviolet exposure time [13] (Reprinted by permission of Elsevier).

The broader, non-uniform area size distribution (a up to 25–36a) predicts an apparent first order behavior, in agreement with the data of Sawunyama et al. [10,11].

We conclude that modeling of stearic acid photocatalyzed disappearance requires knowledge of the initial size distribution of islands. A similar conclusion may apply for the nearly uniform lauric acid ridge width distributions shown in Fig. 6b. Thus modeling

the kinetics of self-cleaning surface removal of organic particulate films requires knowledge of the particle size distribution of the initial deposit. As each size distribution provides its own apparent kinetic order, the modeling task here is daunting.

Future work should also examine photocatalysis on non-uniform titania surfaces. An example is provided recently by Ariedh et al. [13]. These authors found that photocatalyzed attack of a single, thin stearic acid [beta polymorph] crystal (thickness 30–40 nm) grown on a mixed anatase/amorphous titania surface generated flattened hexagonal holes (Fig. 12a diagram), originating at the crystalline anatase microdomains set in the larger amorphous, photo-inactive  $\text{TiO}_2$  surface. The gap distances between parallel planes in these holes increased with UVA illumination time in a zero order fashion (Fig. 12b). Over prior time, other crystal faces, being more reactive, had exhausted earlier, leaving the more stable  $\{h10\}$  and  $\{h11\}$  faces exposed and comprising the boundaries of the growing hole in the SA crystal.

A recent review [14] of photo-induced hydrophilicity of self-cleaning  $\text{TiO}_2$  surfaces concluded that 'no consensus has been reached so far in explaining the exact mechanism of photo-induced hydrophilicity, and a combination of various mechanisms is often required to account for the phenomenon.' As hydrocarbon removal is often associated with hydrophobic to hydrophilic conversion, it is evident that our present analysis rationalizing the removal kinetics of particulate hydrocarbon deposits and our prior analysis of PCO of continuous hydrocarbon films [7] may contribute to mechanistic understanding of photocatalytic self-cleaning surfaces and the associated development of hydrophilicity.

## Acknowledgement

This study was supported by North Carolina State University.

## References

- [1] Y. Paz, A. Luo, L. Ragenberg, A. Heller, J. Mat. Res. 10 (1995) 284.
- [2] A. Mills, A. Lepre, N. Elliott, S. Bhopal, I. Parkin, S.J. O'Neill, J. Photochem. Photobiol. 160 (2003) 213.
- [3] E. Allain, S. Besson, C. Durand, M. Moreau, T. Gacoin, J.P. Boilat, Adv. Funct. Mat. 17 (2007) 549.
- [4] (a) L. Peruchon, E. Puzenat, J.M. Herrmann, C. Guillard, Photochem. Photobiol. Sci. 8 (2009) 1040–1046;  
(b) L. Peruchon, E. Puzenat, A. Girard-Egrot, L. Blum, J.M. Herrmann, C. Guillard, J. Photochem. Photobiol. A: Chemistry 197 (2000) 170–176.
- [5] (a) V. Romeas, P. Pichat, C. Guillard, T. Chopin, C. Lehaut, J. Phys. IV France 9 (1999) 247;  
(b) V. Romeas, P. Pichat, C. Guillard, T. Chopin, C. Lehaut, N. J. Chem. 23 (1995) 365–373.
- [6] A. Zaleska, J. Nalaskowski, J. Hupka, J.D. Miller, Appl. Catal. B: Environ. 88 (2009) 407–412.
- [7] D. Ollis, Appl. Catal. B: Environ. 99 (2010) 478.
- [8] A. Mills, G. Hill, M. Crow, S. Hodgen, J. Appl. Electrochem. 35 (2005) 641–653.
- [9] J.T. Remillard, H.R. McBride, K.E. Nietering, A.R. Drews, X. Zhang, J. Phys. Chem. B 104 (2000) 4440–4447.
- [10] P. Sawunyama, A. Fujishima, K. Hashimoto, Langmuir 15 (1999) 3551.
- [11] P. Sawunyama, L. Jiang, A. Fujishima, K. Hashimoto, J. Phys. Chem. B 101 (1997) 11000.
- [12] M. Ghazzal, B. Barthen, N. Chaoui, App. Catal. B: Environ. 103 (2011) 85.
- [13] F. Araiedh, F. Ducos, A. Houas, N. Chaoui, Appl. Cat. B: Environ. 187 (2016) 350–358.
- [14] S. Banerjee, D.D. Dionysios, S.C. Pillai, Appl. Catal. B: Environ. 176–177 (2015) 396–428.